THE JOURNAL OF BIOLOGICAL CHEMISTRY
Vol. 276, No. 34, Issue of August 24, pp. 32064–32070, 2001

Printed in U.S.A.

The Structure of the Coliphage HK022 Nun Protein-λ-phage *boxB* RNA Complex

IMPLICATIONS FOR THE MECHANISM OF TRANSCRIPTION TERMINATION*

Received for publication, April 4, 2001, and in revised form, May 9, 2001
Published, JBC Papers in Press, May 16, 2001, DOI 10.1074/jbc.M102975200

Cornelius Faber‡§, Manuela Schärpf‡¶, Thomas Becker‡, Heinrich Sticht, and Paul Rösch‖

From the Lehrstuhl für Biopolymere, Universität Bayreuth, Universitätsstr. 30, 95440 Bayreuth, Germany

Nun protein from coliphage HK022 binds to phage *boxB* RNA and functions, in contrast to phage λ N protein, as a transcriptional terminator. The basic Nun-(10–44) peptide contains the *boxB* RNA binding arginine rich motif, ARM. The peptide binds *boxB* RNA and competes with the phage λ ARM peptide N-(1–36) as indicated by nuclear magnetic resonance (NMR) spectroscopy titrations. In two-dimensional nuclear Overhauser enhancement spectroscopy experiments *boxB* RNA in complex with Nun-(20–44) exhibits the same pattern of resonances as it does in complex with N peptides containing the ARM, and we could show that Nun-(20–44) forms a bent α-helix upon binding to the *boxB* RNA. The structure of the *boxB* RNA-bound Nun-(20–44) was determined on the basis of 191 intra- and 30 intermolecular distance restraints. Ser-24 is anchored to the lower RNA stem, and stacking of Tyr-39 and A7 is clearly experimentally indicated. Arg-28 shows numerous contacts to the RNA stem. Leu-22, Ile-30, Trp-33, Ile-37, and Leu-41 form a hydrophobic surface, which could be a recognition site for additional host factors such as NusG. Such a hydrophobic surface area is not present in N-(1–36) bound to *boxB* RNA.

Bacteriophage λ N protein plays an essential role in transcriptional antitermination in the two-phage early operons that are critical for phage development. The inhibition of termination at intrinsic and ρ-dependent terminators by N protein depends on recognition of an RNA element called *nut*[1] (N utilization) on the nascent phage transcript and on four *Escherichia coli* host factors (NusA, NusB, NusG, and ribosomal protein NusE). Together they form a ribonucleoprotein complex that converts the RNA polymerase into a termination-resistant form upon binding (1, 2). N protein binds specifically with high affinity to phage λ *boxB* RNA, a 15-mer RNA hairpin containing a purine-rich pentaloop (3, 4).

Nun protein of phage HK022 is a transcription termination factor that acts, in contrast to other termination factors, highly template- and site-specific. Nun terminates transcription uniquely on phage λ templates (5), competing with λ N protein for a common binding site, nut *boxB* RNA (6). Like N protein, Nun requires additional host factors (NusA, NusB, NusE, and NusG) for efficient termination, whereas the presence of NusA alone inhibits the termination activity of Nun (7). Recently it has been proposed that Nun arrests transcription by anchoring RNA polymerase to DNA (8). Both Nun and N proteins belong to the family of arginine-rich motif (ARM) binding proteins. The structures of phage λ N ARM peptide-*boxB* RNA complexes and of a phage P22 ARM N peptide-*boxB* RNA complex have been solved by NMR (9–12). For both these phage peptides, a very similar mode of binding has been observed, with the peptides bound in the major groove of *boxB* RNA, which adopts a typical hairpin conformation closed by an apical tetraloop.

MATERIALS AND METHODS

Sample Preparation—Unlabeled 15-nucleotide *boxB* RNA was synthesized by *in vitro* transcription using T7 polymerase, a synthetic DNA template (GCCCTTTTTCAGGGCTATAGTGAGTCGTATTA; MWG-BioTech, Ebersberg, Germany), and unlabeled nucleotide triphosphates. The RNA was purified as described previously (12). Freeze-dried *boxB* was resuspended in water, applied on a size exclusion column (NAP, Amersham Pharmacia Biotech) for desalting, and freeze-dried again. Nun-(10–44) and Nun-(20–44) were purchased from Biosyntan (Berlin, Germany). ^{15}N-labeled N-(1–36) peptide was expressed and purified as described previously (12). 1:1 complexes between either Nun-(10–44), Nun-(20–44), or N-(1–36) and *boxB* were generated by addition of small volumes of concentrated (~2 mM) peptide to *boxB* RNA (~0.2 mM). To increase concentration for two-dimensional experiments, Nun-(10–44)-*boxB* RNA complex was freeze-dried and resuspended in 280 μl of H_2O or D_2O, and Nun-(20–44) was concentrated by centricon centrifugation to a final volume of 270 μl. The samples with a concentration of 3 mM and 1.5 mM, respectively, were transferred into Shigemi microtubes.

NMR Spectroscopy—All NMR experiments were recorded at 28 °C for the Nun-(10–44)-*boxB* RNA complex and at 30 °C for the Nun-(20–44)-*boxB* RNA complex on a Bruker DRX 600 spectrometer equipped with ^{1}H/^{13}C/^{15}N probes and triple-axis pulsed field gradient capabilities. For resonance assignment correlated spectroscopy (COSY), total coherence spectroscopy (TOCSY), and nuclear Overhauser enhancement spectroscopy (NOESY) experiments were performed using standard techniques for recording and water suppression (13). For the Nun-(10–44)-*boxB* RNA complex, TOCSY experiments were recorded with 40 and 80 ms mixing time, and NOESY experiments were recorded with 80 and 200 ms mixing time, respectively. For the Nun-(20–44)-*boxB* RNA complex, TOCSY experiments were recorded with a mixing time of 80 ms, and NOESY experiments were recorded with mixing time 150 and 300 ms. ^{1}H^{15}N HSQC spectra were recorded with the fast HSQC pulse scheme (14). All NMR data were analyzed with the NDee (SpinUp Inc., Dortmund, Germany) and XWINNMR (Bruker, Karlsruhe, Germany)

* This project was funded by grants from the Deutsche Forschungsgemeinschaft (Ro617/12-2), the Sonderforschungsbereich 466, and the Bundesministerium für Bildung und Forschung. The costs of publication of this article were defrayed in part by the payment of page charges. This article must therefore be hereby marked "*advertisement*" in accordance with 18 U.S.C. Section 1734 solely to indicate this fact.

‡ The first three authors contributed equally to this work.

§ Present address: Lehrstuhl Experimentalphysik V, Universität Würzburg, Am Hubland, 97074 Würzburg, Germany.

¶ Present address: Dept. of Biochemistry, Univ. of British Columbia, 2146 Health Sciences Mall, Vancouver, British Columbia, Canada V6T 1Z3

‖ To whom correspondence should be addressed: Lehrstuhl für Biopolymere der Universität Bayreuth, Universitätsstr. 30, 95447 Bayreuth, Germany. Tel.: 49-921-553540; Fax: 49-921-553544; E-mail: paul.roesch@uni-bayreuth.de

[1] The abbreviations used are: nut; N utilization; ARM, arginine-rich motif; COSY, correlated spectroscopy; TOCSY, total coherence spectroscopy; NOESY, nuclear Overhauser enhancement spectroscopy; NOE, nuclear Overhauser enhancement; r.m.s.d., root mean square deviation; HSQC, heteronuclear single quantum coherence.

program packages augmented with in-house-written routines. Proton chemical shifts were referenced to external 2,2-dimethyl-2-silapentane-sulfonic acid. The chemical shifts of the ^{15}N resonances were referenced indirectly using the $^{15}N/^{1}H$ Ξ ratio of 0.10132905 of the zero-point frequency at 298 K (15).

Interproton distance restraints were obtained from two-dimensional NOESY spectra of both Nun peptide-*boxB* RNA complexes. NOE intensities were estimated semi-quantitatively on the basis of cross-peak intensities from NOESY spectra collected with 80 ms mixing time. The categories "strong", "medium", and "weak" were converted into distance constraints with upper limit of 2.7, 3.5, and 5.0 Å for peptide intramolecular NOEs (16). For peptide-RNA intermolecular NOEs, these categories were converted in distance constraints with upper limit of 3.0, 4.0, and 5.0 Å, respectively. NOEs that were only visible in the NOESY spectra of Nun-(10–44)-*boxB* RNA complex with 200 ms mixing time were classified as "very weak" with an upper bound of 6.0 Å (10). To improve the convergence of the structure calculation, the lower bounds of all NOE restraints were set to 0 Å (17).

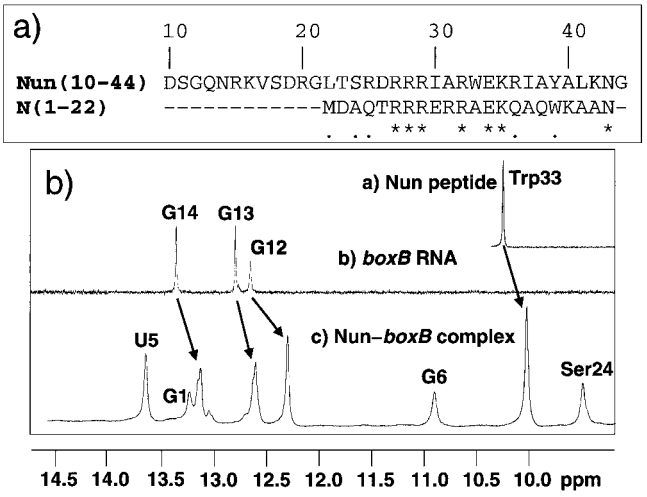

FIG. 1. *a,* alignment of the Nun-(10–44) peptide and phage λ N-(1–22) sequences. *Numbering* is for Nun, *dots* indicate conserved amino acids, and *asterisks* identical amino acids. *b*, one-dimensional NMR spectra of free Nun-(10–44), free *boxB* RNA, and the Nun-(10–44)-*boxB* complex recorded in H_2O/D_2O (9:1), 40 mM NaCl, and 50 mM potassium phosphate, pH 6.4.

Molecular Dynamics Calculations—Experimental data clearly indicate that the *boxB* RNA in the Nun-(10–44) complex is virtually identical to the *boxB* RNA in the N-(1–36) complex. We thus used the structure of the *boxB* RNA in the N-(1–36)-*boxB* RNA complex that we determined earlier (12) (Protein Data Bank entry 1qfq) as a fixed template for all molecular dynamics calculations.

All structure calculations were performed using a modified *ab initio* simulated annealing protocol with an extended version of X-PLOR 3.851 (18). The calculation strategy, which was described in detail previously (19), included floating assignment of prochiral groups (20), a conformational data base potential term (21), and a reduced presentation for non-bonded interactions for part of the calculation (19).

The conformational search phase (60 ps of molecular dynamics at 2000 K) was followed by cooling from 2000 K to 1000 K within 40 ps, concomitantly increasing the force constants for the non-bonded interactions and the angle energy constant for the diastereospecifically unassigned groups to their final values. In the next stage of the calculation, the system was cooled from 1000 K to 100 K within 30 ps, applying the high force constants obtained at the end of the previous cooling stage. To detect the energy minimum, 1200 steps of energy minimization were performed, the final 1000 steps without conformational data base potential. In the final round, 100 structures were calculated, and the 20 structures that showed the lowest energy and the least number of violations of the experimental data were selected for further characterization.

For geometrical analysis and investigation of secondary structure and structural parameters the PROCHECK (22) and NUCPLOT (23) programs were used. Quick visualization and graphical presentation of the structures were performed with the programs RasMol V2.6 (24) and SYBYL 6.5 (Tripos Ass.) (25), respectively. The coordinates were deposited in the Protein Data Bank (entry 1HJI).

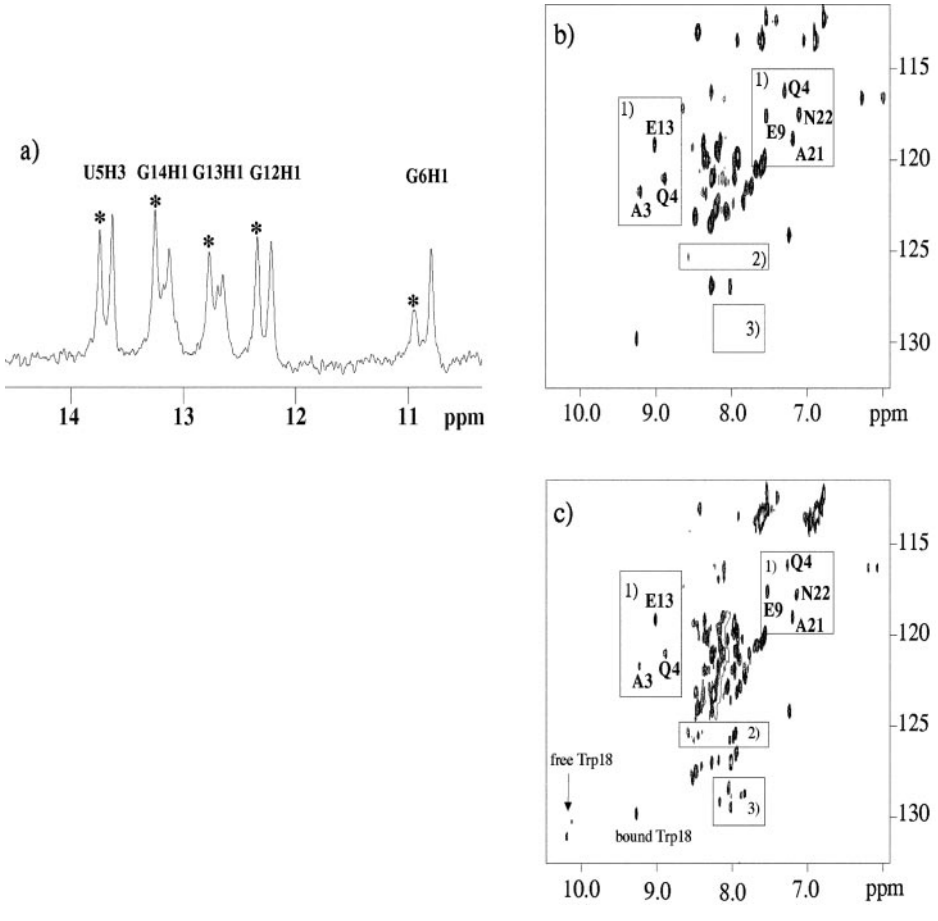

FIG. 2. **Nun-(10–44)-N-(1–36) competition experiments.** All spectra were recorded in H_2O/D_2O (9:1), 40 mM NaCl, and 50 mM potassium phosphate, pH 6.4. *a,* one-dimensional spectrum of the imino protons of *boxB* RNA in presence of Nun-(10–44) and N-(1–36). N-(1–36) was added to the Nun-(10–44)-*boxB* RNA complex, *asterisks* indicate resonances that were observed only after addition of N-(1–36). *b,* HSQC spectrum of N-(1–36) in complex with *boxB* RNA. *c*, HSQC spectrum of N-(1–36) in presence of *boxB* RNA and Nun-(10–44). *Boxes* indicate regions with typical resonances. In box 1 the same resonances as in *b* are observed but with lower intensity; in box 2 resonances typical for free random coil N36 are *highlighted*; and in box 3 new resonances neither observed with free N36 nor in the N36-*boxB* complex are *highlighted*.

RESULTS AND DISCUSSION

One-dimensional NMR Spectroscopy—We have monitored complex formation between the Nun-(10–44) peptide and the 15 nucleotide *boxB* RNA by one-dimensional NMR spectroscopy. Free *boxB* RNA shows three imino proton resonances for G12, G13, and G14. Upon addition of Nun-(10–44) changes in chemical shifts of these resonances were observed, and two additional resonances for the imino protons of U5 and G6 were detected (Fig. 1). The pattern of resonances is identical to that observed for *boxB* RNA in complex with N peptides (11, 12), suggesting that *boxB* RNA adopts virtually identical conformations in the presence of either peptide. Spectra of P22 *boxB* RNA in complex with a P22 N peptide also exhibit an identical pattern of imino proton resonances (10). Structure comparison shows that λ and P22 *boxB* RNA are very similar in complex with their respective N peptides, with one base looped out of the apical pentaloop, allowing formation of a typical GNRA tetraloop structure (10–12). The indole NH resonance of the only Trp residue of N-(1–36), Trp-18, is shifted upfield by more than 1.0 ppm (12) in presence of *boxB* RNA due to its stacking with the aromatic ring of A7, whereas the indole NH resonance of the single Trp residue of Nun-(10–44), Trp-33, is shifted upfield by only 0.2 ppm upon *boxB* RNA complex formation. The comparatively small change in chemical shift for Trp-33 in Nun-(10–44) may be attributed to conformational changes within the peptide upon RNA binding and already suggests that Trp-33 does not stack with A7 of *boxB* RNA. In the spectral range above 9 ppm another new signal is observed, originating from Ser-24 NH. For the N-(1–36)-*boxB* RNA and the P22 N-*boxB* RNA complex a corresponding signal is observed originating from Ala-3 (12) and Ala-2 (10), respectively.

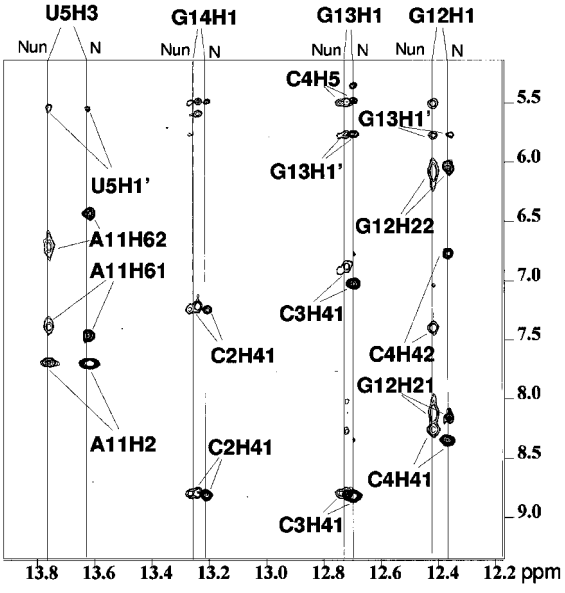

FIG. 3. **Comparison of the NOESY spectra of the Nun-(20–44)-*boxB* RNA complex and the λ N-(1–36)-*boxB* RNA complex in the imino proton resonance region.** λ N-(1–36)-*boxB* RNA complex: H_2O/D_2O (9:1), 10 mM NaCl, 50 mM potassium phosphate, pH 6.5, at 298 K; Nun-(20–44)-*boxB* RNA complex were recorded in H_2O/D_2O (9:1), 10 mM NaCl, 50 mM potassium phosphate, pH 6.4, at 303 K. Pairs of corresponding NOEs are connected by *labeled lines*. All imino resonances of the Nun-(20–44)-*boxB* RNA complex are shifted downfield by 0.05–0.2 ppm compared with the corresponding N-(1–36)-*boxB* RNA complex but exhibit the same cross-peak patterns as the latter complex. All marked NOEs are typical for Watson-Crick base pairs. For G12H1, intraresidual NOEs to the exchangeable amino protons could be observed in both complexes.

Nun-(10–44) and N-(1–36) Bind boxB RNA with Similar Affinities—To compare binding affinities of Nun-(10–44) and N-(1–36) to *boxB* RNA we prepared samples containing *boxB* RNA and equal amounts of Nun-(10–44) and N-(1–36). One-dimensional NMR spectra showed two sets of imino proton resonances with similar intensities, one corresponding to the Nun-(10–44)-bound *boxB* RNA and the other corresponding to the N-(1–36)-bound *boxB* RNA (Fig. 2*a*).

HSQC spectra of ^{15}N-labeled N-(1–36) in complex with unlabeled *boxB* RNA shows a well resolved spectrum (Fig. 2*b*). After addition of an equimolar amount of unlabeled Nun-(10–44) to the N-(1–36)-*boxB* RNA complex several new resonances originating from unbound N-(1–36) appear in the spectrum (Fig. 2*c*), and the resonances of the *boxB*-bound N-(1–36) are reduced to less than 50% of their original intensities. In addition to those resonances from unbound, unstructured N-(1–36), additional resonances that may correspond to a partially structured, but unbound N-(1–36) could be observed. The indole imino proton of Trp-18, for example, shows three resonances: one resonance at 9.2 ppm as observed in the N-(1–36)-*boxB* RNA complex and two resonances around 10.2 ppm, one of which corresponds to the random coil peptide (Fig. 2*c*). As both bound and unbound N-(1–36) are observed regardless whether Nun-(10–44) is added to the N-(1–36)-*boxB* RNA complex or vice versa and as both complexes can be distinguished as N-(1–36) was ^{15}N labeled, we can safely conclude that N-(1–36) and Nun-(10–44) bind to *boxB* RNA with approximately the same affinity and are able to compete with each other.

Two-dimensional NMR Spectroscopy—To obtain further information about the three-dimensional structure of the Nun-(10–44) complex, we recorded homonuclear two-dimensional COSY, TOCSY, and NOESY spectra of the Nun-(10–44)-*boxB* RNA complex and the Nun-(20–44)-*boxB* RNA complex, respectively. The spectra of both complexes for RNA and the

FIG. 4. **Summary of sequential and medium-range NOEs and $C_\alpha H$ chemical shift index (HαCSI) of Nun-(20–44) in the *boxB* RNA complex.** The width of the horizontal bars indicates the relative NOE strengths, categorized by cross-peak intensity as strong, medium, and weak. Positive and negative chemical shift indices are indicated by *bars above* and *below* the axis, respectively. Positive chemical shift indices typify regions with β-sheets, and negative chemical shift indices typify regions with α-helix. The secondary structure assignments are depicted in the *bottom line*.

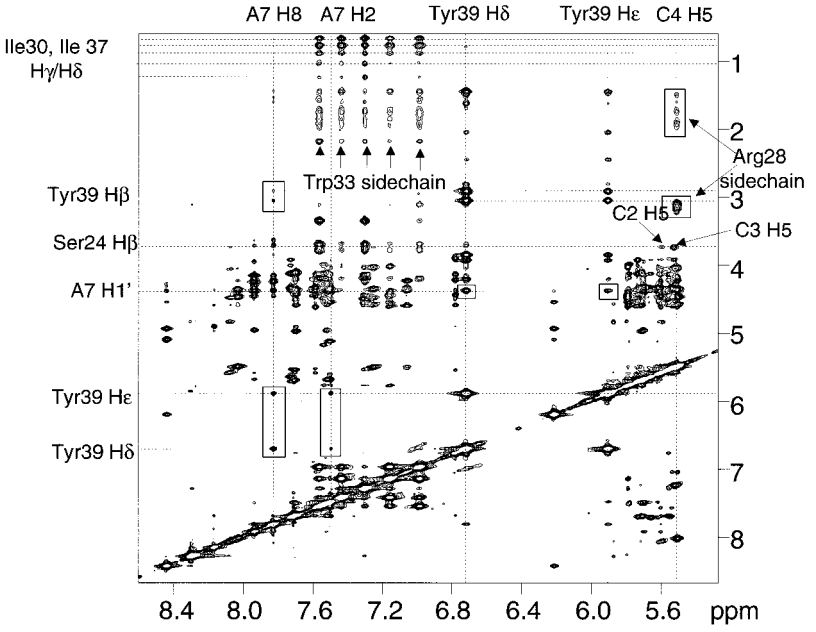

FIG. 5. **NOESY spectrum of the Nun-(10–44)-*boxB* RNA complex, recorded with 200 ms mixing time in 40 mM NaCl, 50 mM potassium phosphate, pH 6.4.** Resonances of protons showing key NOEs are labeled. Several intermolecular NOEs between A7 and Tyr-39 and C4H5 and Arg-28, respectively, are *boxed*. NOEs between Ser-24 and C3H5 as well as C2H5 are indicated by *arrows*. Aromatic protons of Trp-33 show prominent NOE peak ladders which could be assigned to either Ile-30 or Ile-37, which are involved in forming a hydrophobic surface. Additional intermolecular NOEs between Nun-(10–44) aliphatic protons and A7H8 are visible.

TABLE I
Experimental restraints for the final structure calculation

Results of the structure calculations. Experimental restraints and simulated annealing statistics are summarized. r.m.s.d. values are averages over a family of 20 converged structures. Values in *parenthesis* indicate the standard deviation from this mean.

NOEs	
Total	221
Peptide-intramolecular	
total	191
sequential ($\|i-j\|=1$)	98
medium range ($\|i-j\|<5$)	93
long range ($\|i-j\|\geq 5$)	0
intraresidual	0
Peptide-RNA: intermolecular	30

Restrained simulated annealing statistics	
r.m.s.d. from experimental NOEs (Å)	0.0136 (±0.0024)
r.m.s.d. from ideal bond lengths (Å)	0.002274 (±0.000025)
r.m.s.d. from ideal bond angles	0.576 (±0.004)
Atomic r.m.s.d. of 20 best structures (Å)	
Peptide only in complex, residues 22–43	backbone: 0.52; all heavy atoms: 1.36
Peptide only in complex, residues 20–44	backbone: 0.94; all heavy atoms: 1.91
Peptide + RNA, residues 22–43	backbone: 1.1; all heavy atoms: 1.76
Peptide + RNA, residues 20–44	backbone: 1.6; all heavy atoms: 2.4

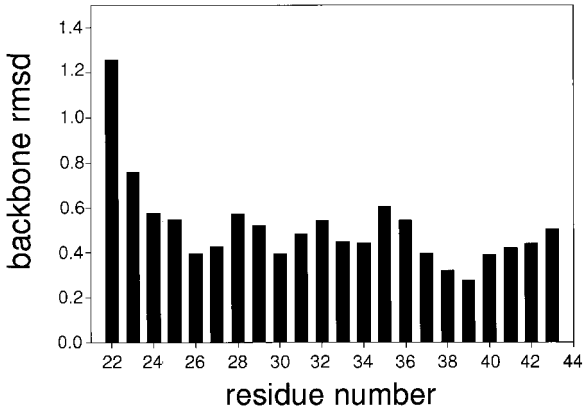

FIG. 6. **Structure calculation of Nun-(20–44)-*boxB* complex.** The backbone r.m.s.d. of Nun-(20–44) as complexed with nut *boxB* RNA is plotted against the residue number for residues 22–43.

peptide sequence from Leu-22 to Asn-43 were highly similar. Sequence-specific backbone assignments for Nun-(10–44)-*boxB* RNA complex as well as Nun-(20–44)-*boxB* RNA complex could be performed completely.

Assignment of RNA Protons and Verification of the RNA Fold—In two-dimensional spectra all H6/H8, H1′, pyrimidine H5, and cytosine amino protons could be assigned. Pyrimidine H5 and H6 were identified in two-dimensional COSY-spectra, cytidine amino protons could be assigned by intraresidual NOEs to their own H5, and purine H8 and all H1′ were assigned by comparison with spectra of *boxB* RNA in complex with λ N-(1–36). In this way, putative assignments were also possible for some isolated ribose resonances in the loop region, which show characteristic upfield (A7) or downfield (A9) shifts. Adenine H2 could be assigned for A7 and A9, and A11H2 could be identified by the strong NOE to U5H3 (Fig. 3).

NOEs indicating formation of Watson-Crick base pairs were observed for C2:G14, C3:G13, C4:G12, and U5:A11. Comparison of the Nun-(20–44)-*boxB* RNA and the λ N-(1–36)-*boxB* RNA NOESY spectra in the region of the imino protons show that the imino protons in Nun-(20–44)-*boxB* RNA are shifted downfield by about 0.05–0.2 ppm, whereas for all non-exchangeable protons no systematic change of the chemical shifts between the spectra could be observed (Fig. 3). Both spectra show an identical pattern of resonances suggesting virtually identical folds in the stem region.

The connectivities between the ribose and their own as well as their sequentially neighboring base were obtained from $H1'_i$-H6/H8$_i$ and $H1'_i$-H6/H8$_{i+1}$-NOEs (26). As in the spectra of λ N-(1–36)-*boxB* RNA, no $H1'_i$-H6/H8$_{i+1}$-NOE could be observed between A8 and A9. This and unusual downfield shifts of the resonances of A9 in the *boxB*-RNA complexes of both peptides suggest that A9 is looped out the Nun-(10–44) complex in a fashion virtually identical to that observed in the N-(1–36)-*boxB* RNA complex. Spatial vicinity of A8 and A10 as in λ N-(1–36)-*boxB* RNA complex is possible, but the corresponding NOEs could not be assigned unambiguously due to frequency degeneration. Finally, extreme upfield shifts of U5H5 and A7H1′ resonances that were also observed in the λ N-(1–36)-*boxB* RNA complex lead to the conclusion that *boxB* RNA adopts a highly similar structure in complex with either Nun-(20–44) or λ N-(1–36).

Assignment of Peptide Protons—For Nun-(10–44) strong TOCSY and relatively weak NOESY signals were observed for the first 10 residues in the complex, suggesting that this region

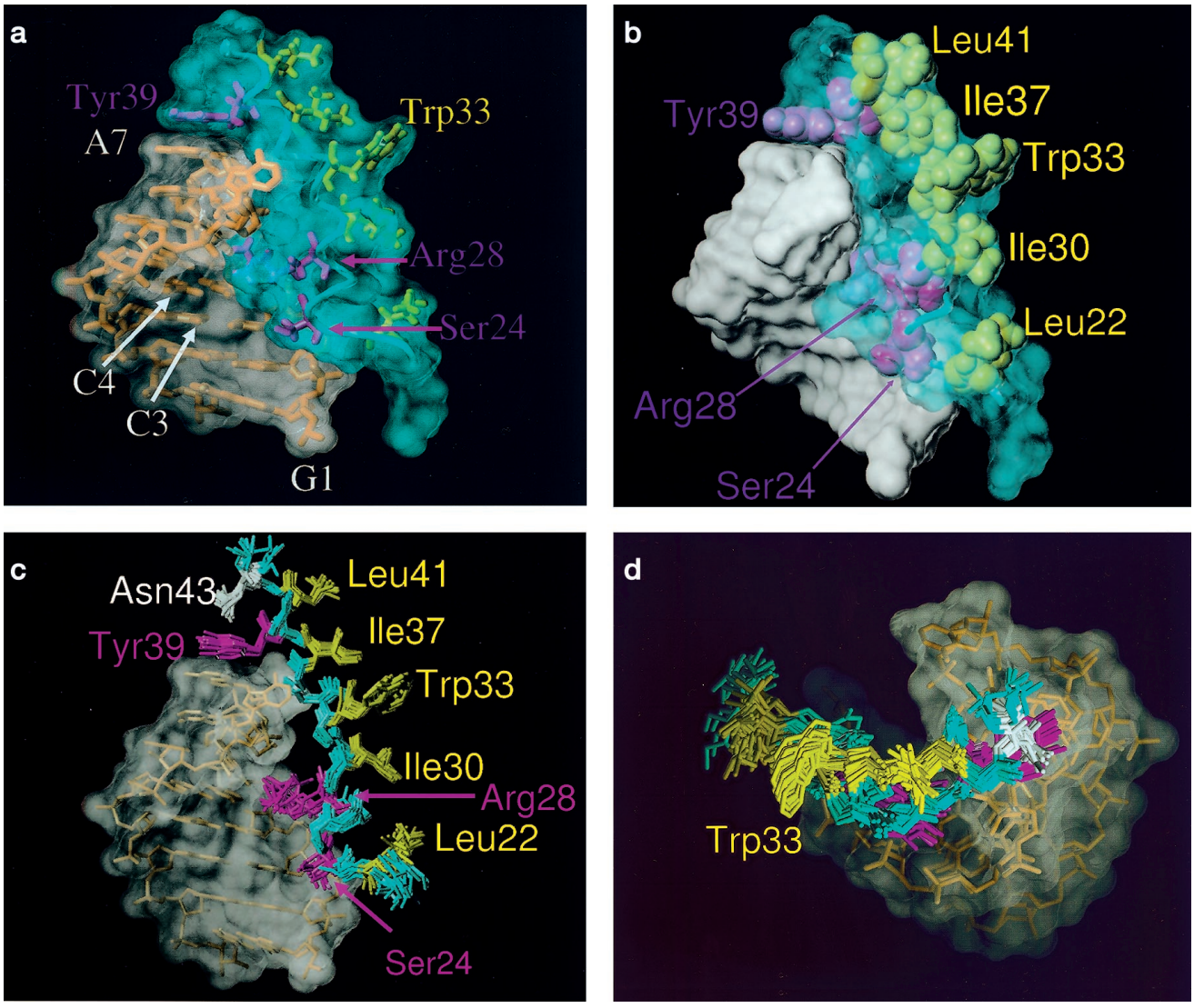

FIG. 7. *a*, lowest energy structure of the Nun-(20–44)-*boxB* RNA complex. RNA surface, *gray*; peptide Conolly surface, *light blue*; RNA, *orange*; peptide backbone, *cyan*; peptide residues interacting with the RNA (Ser-24, Arg-28, Tyr-39), *magenta*; residues forming a hydrophobic surface (Leu-22, Ile-30, Trp-33, Ile-37, Leu-41), *yellow*. The peptide is bound tightly in the major groove of the RNA forming a bent α-helix. Tyr-39 stacks on A7, Ser-24 is bound between C2 and C3, and Arg-28 contacts the bases of C4 and U5. *b*, as in *a:* RNA surface, *gray*; peptide Conolly surface, *light blue translucent;* peptide backbone, *cyan*; peptide residues represented as *sticks* in *a* are shown in *spacefill* mode. The complex structure is very compact with no cavities found between molecules. Hydrophobic residues are located at the solvent exposed side opposite to the peptide-RNA interface to form a hydrophobic patch. *c,* overlay of the 20 structures with the lowest overall energy. RNA, as in *a:* peptide, *cyan*; hydrophobic side chains as part of the hydrophobic surface patch, *yellow*; other hydrophobic side chains, *magenta*; Asn-43, *white*. A7, Tyr-39, and Asn-43 exhibit the same structural characteristics as A7, Trp-18, and Asn-22 in the N-(1–36)-*boxB* RNA complex, with Asn-43 packing upon the Tyr-39 aromatic side chain which, in turn, is stacking upon A7. Residues contacting the RNA and forming the hydrophobic surface, respectively, are very well defined. *d*, the hydrophobic residues form a structure that resembles a sharp ridge which may serve as a recognition site for additional host factors.

is flexible and is not involved in RNA binding. Nun-(10–44) and Nun-(20–44) showed identical chemical shifts for the overlapping peptide. Thus, all further experiments were performed using Nun-(20–44).

For the Nun-(20–44) peptide-*boxB* RNA complex the sequence-specific resonance assignments could be performed by standard two-dimensional NMR methods (27). NOESY cross-peaks in the backbone amide-amide region indicated the presence of helical structures for a large part of the RNA bound peptide. Unambiguous assignments of the amino acid side chain protons could be performed for all amino acids except Arg-25, Arg-27, Arg-29, Arg-32, Arg-36, and Lys-35 due to frequency degeneration and missing COSY-cross-peaks in the $C_\alpha H$ region. Some arginine $C_\beta H$ could be assigned using the helix-typical $d_{\alpha\beta}(i, i + 3)$ cross-peaks.

Nun-(20–44) Forms a Helix in the Complex—The analysis of the $C_\alpha H$ chemical shift index (28) gave first evidence for a helical structure from Ser-24 to Asn-43. For this region, helix-typical $(i, i + 3)$ and $(i, i + 4)$ NOEs could be observed throughout the sequence (Fig. 4), in agreement with the observation of only very weak cross-peaks in the TOCSY-spectra for Leu-22 and subsequent residues, probably due to very small $^3J_{HN\alpha}$ coupling constants.

NOE Assignment and Structure Determination—To resolve ambiguities in NOE assignments, an iterative procedure for structure calculation was performed. Initially, only those NOEs that could be assigned unambiguously were used for molecular dynamics calculations. By verification of the resulting structures additional NOEs could be assigned, for example NOEs from the Trp-33 aromatic side chain (Fig. 5) to either Ile-30 or Ile-37.

Intermolecular NOEs—30 intermolecular NOEs could be identified unambiguously in the NOESY spectra. For the β-protons of Ser-24 the same NOEs with C2 and C3 are observed as

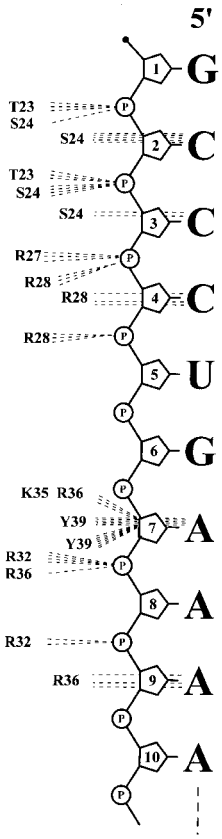

FIG. 8. **Schematic representation of hydrophobic and electrostatic interactions between Nun-(20–44) peptide and *boxB* RNA.** Only nucleotides 1–10, which are directly involved in contacts with the peptide, are shown. Bases are in *gray*, phosphate groups are represented by *small circles*, and sugar moieties are represented by *pentagons*. Intermolecular electrostatic and hydrophobic interactions determined by analysis of the structures with NUCPLOT are indicated by *dashed lines*.

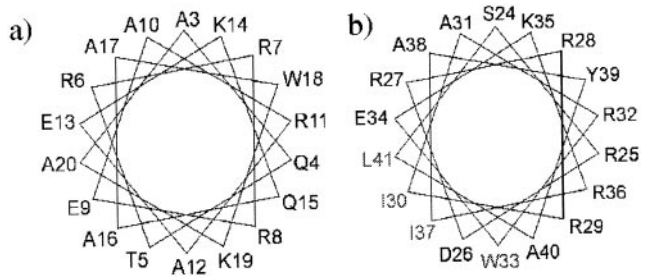

FIG. 9. **Helical wheel representation of N-(3–20) (*a*) and Nun-(24–41) (*b*).** In *b*, hydrophobic residues with large side chains are in *gray*. They are all exposed at one side. Corresponding residues in *a* are either charged or alanines.

for the β-protons of Ala-3 in the N-(1–36)-*boxB* complex. The aromatic protons of Tyr-39 show the same NOEs with A7 as observed for the aromatic protons of Trp-18 in the N-(1–36)-*boxB* complex (12). Further, NOEs between C4H5, U5H5, and side chain protons of Arg-28 which correspond to C4-Arg-7 NOEs in the N-(1–36)-*boxB* RNA complex could be assigned (Fig. 5).

Quality of the Nun-(20–44) Peptide-boxB RNA Complex Structure—The final structure was calculated based on a total number of 191 intra- and 30 intermolecular distance restraints. A subset of 20 structures with energies lower than 182 kcal·mol^{-1} out of 120 structures was selected for further analysis. None of these structures showed NOE violations larger than 0.13 Å (Table I.).

The backbone of the peptide bound to *boxB* RNA is well defined for residues 22–43, with a backbone root mean square deviation (r.m.s.d.) of 0.52 Å. Residues 20, 21, and 44 remain disordered so that inclusion of these residues in the r.m.s.d. calculation increases the backbone r.m.s.d. to 0.94 Å. COOH-terminal residues and residues forming the hydrophobic surface show the lowest r.m.s.d./residue (Fig. 6) (<0.5 Å) indicating that the structure is very well defined in these regions.

Structural Features of the Nun-(20–44)-boxB RNA complex—PROCHECK analysis of Nun-(20–44) in complex with *boxB* RNA shows that in the 20 accepted structures 95.9% of the residues are found in the most favored regions, 3.9% in the allowed regions of the Ramachandran plot. The Nun peptide forms an α-helix for residues 24–43, which is bent at residues Ala-31 and Arg-32. Bending does not require deviations from ideal helix Φ/Ψ angles. The COOH terminus of the peptide is well defined by contacts between Asn-43 and Tyr-39, reflected by several NOEs between side chain protons of both amino acids (Figs. 5 and 7). In the complex, Tyr-39 stacks tightly on A7 anchoring Nun-(20–44) to the RNA, and the γ-amino group of Asn-43 packs on the aromatic ring of Tyr-39 (Fig. 7*a*). The same structural characteristics are exhibited in the N-(1–36)-*boxB* RNA complex by A7, Trp-18, and Asn-22 (12).

The NH_2-terminal residues occupy a well defined position close to C3, reflected by the intermolecular NOEs observed between the bases of both C2 and C3 and Ser-24. Arg28 is in close contact to the bases of C4 and U5, which is shown by several NOEs.

According to the NUCPLOT analysis of the 20 converging structures, additional residues critical for the RNA recognition are Arg-27, Arg-32, Arg-36, and Lys-35, which are involved, as well as Arg-28, in numerous electrostatic and hydrophobic contacts (Fig. 8) with the phosphate backbone and the sugar moieties. In several structures, hydrophobic contacts between the looped out base of A9 and Arg-36 are observed. Arg-36 occupies the position of Gln-15 in λ N contacting the bases of A7 and A8 in the N-(1–36)-*boxB* RNA complex.

The most distinguishing feature of the Nun-(20–44)-*boxB* RNA structure is the formation of a hydrophobic, solvent-exposed surface. The wheel representation of the Nun-(20–44) helix in the *boxB* RNA complex clearly indicates that this helix is amphipathic, and all hydrophobic residues with large side chains are exposed to one side. Corresponding residues of N-(1–36) are either charged or alanines (Fig. 9).

Various NOEs have been assigned between Trp33 aromatic side chain protons and aliphatic protons of Ile-30 and Ile-37. In the D_2O-NOESY spectra, an NOE between methyl protons of Leu-41 and Ile-37 could be observed. Additionally, the Leu-22 side chain is in spatial vicinity to Ile-30 and also contributes to the hydrophobic surface (Fig. 7*b*). All these residues are well defined in the structure calculations as shown in the overlay of 20 structures with the lowest overall energy (Fig. 7*c*). The network of hydrophobic residues forms a clear cut ridge (Fig. 7*d*) suggesting that the N-*boxB*- and the Nun-*boxB*-RNA complexes are recognized by different mechanisms by the target host cell factors.

It has been shown that NusA binds to the COOH-terminal region of Nun and that NusA alone without the other Nus factors inactivates Nun function as a terminator (7). NusA binding to *boxB* RNA can be nearly abolished by mutation of looped out nucleotide A9 (29). Together with N protein, NusA strongly enhances antitermination, which is also strongly reduced *in vivo* by mutations of A9 (30) implying that A9 plays a crucial role in antitermination. The current work thus may serve as a basis for the design of specific peptide and RNA mutants aimed at a better understanding of the crucial termi-

nation/antitermination regulation of the viral replication on a structural level.

Acknowledgment—We gratefully acknowledge excellent technical assistance by Ulrike Herzing.

REFERENCES

1. Das, A. (1993) *Annu. Rev. Biochem.* **62,** 893–930
2. Greenblatt, J., Nodwell, J. R. & Mason, S. W. (1993) *Nature* **364,** 401–406
3. Franklin, N. C. (1984) *J. Mol. Biol.* **181,** 75–84
4. Lazinski, D., Grzadzielska, E. & Das, A. (1989) *Cell* **59,** 207–218
5. Robert, J., Sloan, S. B., Weisberg, R. A., Gottesman, M. E., Robledo, R. & Harbrecht, D. (1987) *Cell* **51,** 483–492
6. Chattopadhyay, S., Hung, S. C., Stuart, A. C., Palmer, A. G., III, Garcia-Mena, J., Das, A. & Gottesman, M. E. (1995) *Proc. Natl. Acad. Sci. U. S. A.* **92,** 12131–12135
7. Watnick, R. S. & Gottesman, M. E. (1998) *Proc. Natl. Acad. Sci. U. S. A.* **95,** 1546–1551
8. Watnick, R. S. & Gottesman, M. E. (1999) *Science* **286,** 2337–2339
9. Su, L., Radek, J. T., Hallenga, K., Hermanto, P., Chan, G., Labeots, L. A. & Weiss, M. A. (1997) *Biochemistry* **36,** 12722–12732
10. Cai, Z., Gorin, A., Frederick, R., Ye, X., Hu, W., Majumdar, A., Kettani, A. & Patel, D. J. (1998) *Nature Struct. Biol.* **5,** 203–212
11. Legault, P., Li, J., Mogridge, J., Kay, L. E. & Greenblatt, J. (1998) *Cell* **93,** 289–299
12. Schärpf, M., Sticht, H., Schweimer, K., Boehm, M., Hoffmann, S. & Rösch, P. (2000) *Eur. J. Biochem.* **267,** 2397–2408
13. Cavanagh, J., Fairbrother, W. J., Palmer, A. G., III & Skelton, N. J. (1996) *Protein NMR spectroscopy*. Academic Press, San Diego, CA
14. Mori, S., Abeygunawardana, C., O'Neil-Johnson, M. & van Zijl, P. C. M. (1995) *J. Magn. Reson. B* **108,** 94–98
15. Live, D. H., Davis, D. G., Agosta, W. C. & Cowburn D. (1984) *J. Am. Chem. Soc.* **106,** 1939–1941
16. Clore, G. M., Gronenborn, A. M., Nilges, M. & Ryan, C. A. (1987) *Biochemistry* **26,** 8012–8023
17. Varani, G., Aboul-ela, F. & Allain, F. H.-T. (1996) *Prog. Nuc. Magn. Res. Spec.* **29,** 51–127
18. Brünger, A. T. (1996) *X-PLOR,* Version 3,851. online, Howard Medical School & Yale University, New Haven, CT
19. Nilges, M., Gronenborn, A. M., Brünger, A. T., Clore, G. M. (1988) *Protein Eng.* **2,** 27–38
20. Holak, T. A., Nilges, M. & Oschkinat, H. (1989) *FEBS Lett.* **242,** 218–224
21. Kuszewski, J., Gronenborn, A. M. & Clore, G. M. (1996) *Protein. Sci.* **5,** 1067–1080
22. Laskowski, R. A., MacArthur, M. W., Moss, D. S. & Wright, P. E. (1993) *J. Appl. Crystallogr.* **26,** 283–291
23. Luscombe, N. M., Laskowski, R. A. & Thornton J. M. (1997) *Nucleic Acids Res.* **25,** 4940–4945
24. Sayle, R. (1995) *RasMol V 2.6. Molecular Visualisation Program*. Glaxo Wellcome Research and Development, Stevevage, Hertfordshire, U. K.
25. *SYBYL,* Version 6.5, Tripos Inc., St. Louis, MO
26. Varani, G. & Tinoco, I. Jr. (1991) *Q. Rev. Biophys.* **24,** 479–532
27. Wüthrich, K. (1986) *NMR of Proteins and Nucleic Acids*, John Wiley & Sons Inc., New York
28. Wishart, D. S., Sykes, B. D. & Richards, F. M. (1992) *Biochemistry* **31,** 1647–1651
29. Mogridge, J., Mah, T-F. & Greenblatt, J. (1995) *Genes Dev.* **9,** 2831–2844
30. Chattopadhyay, S., Garcia-Mena, J., DeVito, J., Wolska, K. & Das, A. (1995) *Proc. Natl. Acad. Sci. U. S. A.* **92,** 4061–4065